V

Publication V

Niskanen, A.J., Ylinen-Hinkka, T., Kulmala, S., Franssila, S., Integrated microelectrode hot electron electrochemiluminescent sensor for microfluidic applications, *Sensors and Actuators B: Chemical* **152** (2011) 56–62.

Sensors and Actuators B 152 (2011) 56–62

Contents lists available at ScienceDirect

Sensors and Actuators B: Chemical

journal homepage: www.elsevier.com/locate/snb

Integrated microelectrode hot electron electrochemiluminescent sensor for microfluidic applications

A.J. Niskanen[a,b,*], T. Ylinen-Hinkka[c], S. Kulmala[c], S. Franssila[a]

[a] Department of Materials Science and Engineering, Aalto University School of Science and Technology, P.O. Box 16200, FI-00076 Aalto, Finland
[b] Department of Micro and Nanosciences, Aalto University School of Science and Technology, P.O. Box 13500, FI-00076 Aalto, Finland
[c] Laboratory of Analytical Chemistry, Aalto University School of Science and Technology, P.O. Box 16100, FI-00076 Aalto, Finland

ARTICLE INFO

Article history:
Received 2 June 2010
Received in revised form 7 September 2010
Accepted 21 September 2010
Available online 1 October 2010

Keywords:
Electrochemiluminescence
Chemiluminescence
Thin insulating film-coated electrodes
Integrated microelectrodes
Microfluidic chip

ABSTRACT

Electrochemiluminescence using insulator-covered electrodes to tunnel emit hot electrons into solution is a sensitive and selective method of quantitative chemical analysis. Immunoassays can be performed by binding antibodies to the working electrode surface, and labeling the secondary antibody or analyte with luminophores. In this paper we present a miniaturized hot electron-induced electrochemiluminescence device with sub-nanomolar detection limits, where both the working electrode and counter electrode are integrated into a single chip. Microfluidics are fabricated in polydimethylsiloxane elastomer, or fluid confinement by patterned hydrophobic areas are integrated into the same device. Devices are processed on both silicon and glass substrates, using either oxidized silicon, or aluminum thin films covered by atomic layer deposited alumina, as the working electrodes. Different electrode geometries are compared in terms of detection efficiency and luminescence uniformity.

1. Introduction

Hot or hydrated electrons are extremely strong reducing species which can produce a wide variety of electrochemical reactions in aqueous solution. They can be produced by methods such as pulse radiolysis [1–3] or photoionization [4,5], but a more convenient method is tunnel emission during a cathodic pulse, from conductive electrodes covered by a thin insulating film [6–8]. During a high-amplitude cathodic pulse, electrons are tunnel emitted with low loss of energy through the insulator and into the solution, and achieve an energy higher than the conduction band edge of water (hot electrons), and may subsequently be thermalized and solvated on a femtosecond time scale by the surrounding water molecules (hydrated electrons). In either case, they remain as excess electrons in water, prior to reducing another solvated species, or in high concentrations forming a solvated electron pair, which reacts rapidly with water to form hydrogen. In lower concentrations, the single hydrated electron has been shown by pulse radiolysis studies to be very unreactive with water [9], and can therefore be used to initiate high-energy electrochemical reactions with dissolved species. Higher-energy reactions are possible than at ordinary active metal electrodes, where the achievable potential is limited by the breakdown of water [6], but from a practical point of view, the method is very similar to electrochemistry with ordinary conductive electrodes.

One application of hot electron electrochemistry is quantitative analysis by hot electron-induced electrochemiluminescence (HECL). Here the concentration of luminophores in sample solution can be determined by their luminescence excited by the hydrated electrons [6]. If antibodies are bound to the working electrode surface, an immunoassay can be realized using luminophores as labels to be detected by HECL [10].

A variety of dielectrics of various thicknesses have been previously tested in the working electrode, either over highly conductive silicon [11] or over thin film metal electrodes [12], using a separate platinum wire as the counter electrode. A plastic sample cell, mechanically sealed against the electrode surface, has been used for sample containment. In the current work, the counter electrode has been fabricated onto the working electrode's surface, and a sample chamber is formed on the chip by bonding a cast-molded polydimethylsiloxane (PDMS) lid to the electrode chip. This makes a fully integrated HECL sample cell which is convenient to use, and as it is fully disposable, it also eliminates the risk of sample cross-contamination. Thus the device as such is usable in point-of-care analytical applications.

Since PDMS has high optical transparency over the wide wavelength range of 240–1100 nm, and is electrically insulating and chemically inert towards most reagents [13–15], it has been

* Corresponding author at: Department of Materials Science and Engineering, Aalto University School of Science and Technology, P.O. Box 16200, FI-00076 Aalto, Finland. Tel.: +358 9 470 22319; fax: +358 9 470 26080.
E-mail address: Antti.Niskanen@tkk.fi (A.J. Niskanen).

0925-4005/$ – see front matter © 2010 Elsevier B.V. All rights reserved.
doi:10.1016/j.snb.2010.09.049

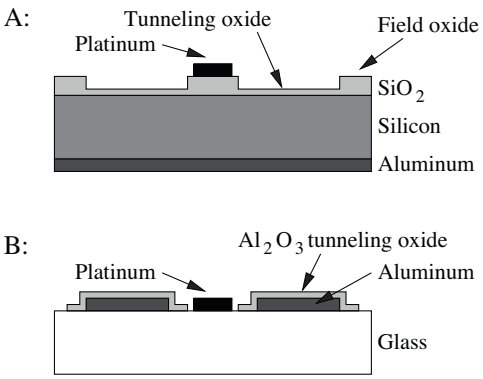

Fig. 1. Cross-sectional views of silicon (A) and glass (B) devices. Vertical and lateral dimensions are not to scale.

widely used in integrated microanalytical systems with optical detection. Published applications include immunoassays with fluorescent detection [16], isoelectric focusing with chemiluminescent detection [17], capillary electrophoresis or flow injection analysis with conventional anodic electrochemiluminescent (ECL) detection [18–20] and DNA quantification on magnetic microbeads with anodic ECL [21]. Other biomedical applications which could benefit from HECL detection are those involving polymerase chain reaction amplification of DNA fragments, a field which has lately seen much progress in miniaturization, often using PDMS in its microfluidic systems [22,23]. Since the present HECL device with its PDMS sample chamber is fabricated by basically the same methods as these PDMS microfluidic systems, it also serves as a proof-of-concept for the integration of HECL detection into such systems. Compared to anodic ECL, HECL offers several advantages including higher excitation energy [6] and simultaneous excitation of multiple luminophores enabling multianalyte detection or internal standards [24].

An alternative sample containment scheme, utilizing patterned hydrophobic films, is also presented. While PDMS fluidics are easily fabricated in volume using a single master mold, the bonding of the PDMS cover to the HECL chip is a major extra fabrication step, whether done on the chip or wafer scale. Hydrophobic surface modification, on the other hand, is a simple wafer-scale deposition step, and patterning is readily effected by a single photolithographic step and lift-off.

The current HECL devices are fabricated using thermally oxidized silicon as the working electrode and platinum thin film counter electrodes, and they attain sub-nanomolar sensitivity to the terbium(III) chelate used as the model analyte. A glass device with sputtered aluminum thin films coated with atomic layer deposited (ALD) alumina as the working electrode, is also tested to demonstrate the feasibility of deposited electrodes on insulating substrates. Various electrode geometries are investigated and assessed in terms of HECL signal intensity and luminescence uniformity over the working electrode.

2. Experimental

2.1. Silicon device fabrication

Devices with oxide covered silicon working electrodes were fabricated from *n*-type silicon wafers of 0.005–0.018 Ω cm resistivity and (1 1 1) orientation. The wafers were initially RCA-cleaned with SC-1 (NH_4OH/H_2O_2 solution at 80 °C), dilute HF, then SC-2 (HCl/H_2O_2 solution at 80 °C) and wet oxidized at 950 °C for 90 min to yield 380 nm field oxide thickness. The oxide was patterned by standard optical lithography and wet etching to define the working electrode areas. Following RCA-cleaning with HF-dip last to remove any native oxide, the thin tunneling oxide of the working electrode was grown by dry oxidation in 10% oxygen at 850 °C. Approximately 4 nm of oxide was grown in 20 min. Following photolithography, 50 nm of platinum was deposited by sputtering and patterned by lift-off. Electrical contact to the platinum counter electrode is made through contact pads (connected in parallel) on the front of the wafer, while the silicon working electrode is contacted through the wafer backside. Although not always found necessary, the backside contact could be improved by wet etching the wafer backside free of oxide, and sputtering onto it approximately 100 nm of aluminum. Fig. 1A presents a schematic cross-sectional view across a WIRE type device (detailed in Section 2.3).

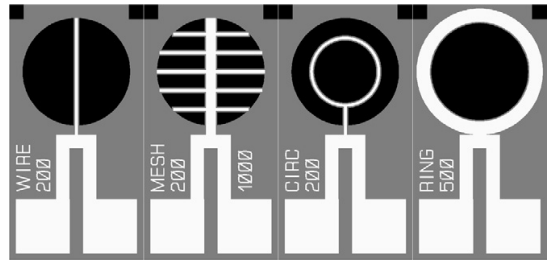

Fig. 2. Some of the electrode geometries tested in silicon devices. Black and white areas represent the working and counter electrodes, respectively. Gray areas are insulation. Indicated on the chip are the electrode type (WIRE, MESH, CIRC, or RING), linewidth of the counter electrode (200 μm in the first three) and counter electrode line spacing in the MESH devices (1000 μm version is shown).

2.2. Glass device fabrication

Pyrex glass wafers were initially cleaned with SC-1, and 400 nm of aluminum was sputtered to form the working electrodes, and to serve as a sacrificial layer in the patterning of platinum. First the counter electrode areas were defined by standard optical lithography, and aluminum was removed from those areas by wet etching. The aluminum film was intentionally overetched by 100% to form an overhang structure in the photoresist, which was not removed at this stage. Platinum was then sputtered and patterned by lift-off, facilitated by the overhanging resist. Next the aluminum working electrodes were defined by lithography and wet etching. About 4 nm of aluminum oxide was deposited by ALD from trimethylaluminum and water precursors at 220 °C temperature. This layer was removed from the platinum counter electrode and contact pads by photolithography and etching. Etching was effected by the alkaline photoresist developer solution during 2 min of overdevelopment, which the photoresist pattern easily withstands. Finally the photoresist was removed. Electrical contact is made to both the working and counter electrodes through their respective contact pads on the front of the wafer. A schematic cross-section of a glass device is shown in Fig. 1B.

2.3. Electrode geometry

Several counter electrode geometries were investigated on both glass and silicon devices. Fig. 2 presents some of the silicon designs. Black areas in the figure represent the silicon working electrode covered by the silicon dioxide tunneling dielectric, white areas represent platinum metalization for the counter electrode, while gray areas represent the thick field oxide for electrical insulation. Electrode designs included simple wires running across the working

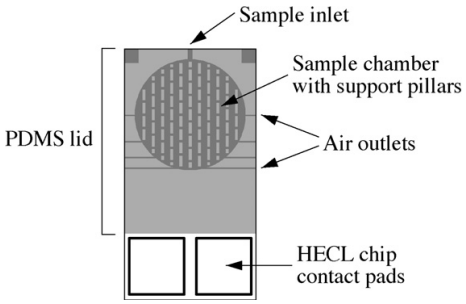

Fig. 3. The PDMS capillary-filling sample chamber.

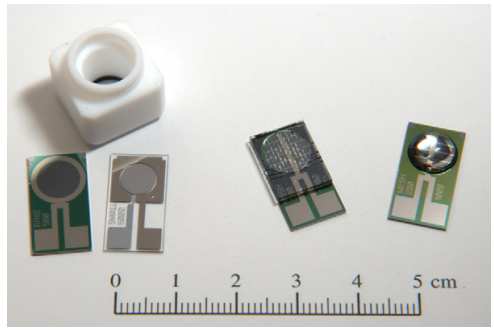

Fig. 4. Planar silicon and glass electrode chips and the PTFE sample cell (left), a silicon device with a capillary-filling PDMS chamber (middle), and a silicon device with a hydrophobically confined sample droplet (right).

electrode (Fig. 2, WIRE), meshes of wires spread across the working electrode (Fig. 2, MESH), circular counter electrodes within the working electrode area (Fig. 2, CIRC), and ring-shaped counter electrodes fully enclosing the round working electrode (Fig. 2, RING). The linewidth of the counter electrode was varied, as well as the density of lines in the MESH designs. In all designs, a minimum of 100 μm spacing (insulated by the thick field oxide) was left between the working and counter electrodes. Similar geometries were tested on glass devices.

2.4. PDMS fluidics

A master mold for casting PDMS was fabricated on a silicon wafer by processing SU-8 structures on its surface by standard photolithographic techniques. A 50 μm layer of SU-8 50 or a 350 μm layer of SU-8 100 was used for these devices. Multiple layers of SU-8 could be used to create thicker or multi-level structures. Once complete, the master was coated with a 30 nm film of anti-sticking Teflon-like fluoropolymer from a CHF_3 plasma in an Oxford PlasmaLab-80+ reactive ion etching system, using 100 sccm flow rate and 50 W RF power. This facilitates easier peeling of the cured PDMS from the master, and prolongs the master's lifetime, without affecting the bonding properties of the PDMS.

The PDMS fluidic chip was fabricated by casting Sylgard 184 silicone elastomer, base and curing agent mixed in a 10:1 ratio, onto the master mold in a Petri dish. The wet PDMS was then outgassed in vacuum and cured at 50 °C for 2 h. The cured PDMS was peeled off the master, cut into individual chips, and bonded to the HECL electrode chips. Bonding was improved by first exposing both the PDMS fluidic chip and the HECL electrode chip to oxygen plasma in a Technics Plasma TePla-400 reactor for 30 s, using 800 sccm oxygen flow and 800 W RF power. This plasma treatment also makes the PDMS surface hydrophilic, enabling filling of the sample chamber by capillary force.

Fig. 3 shows the geometry of the PDMS lid: An inlet channel at one end of the chip is used to fill the chamber by dipping the chip's edge in sample solution, while multiple channels allow air to escape during filling. Small pillars support the chamber's PDMS ceiling. In the current design, the pillars are evenly distributed throughout the fluidic chamber, not optimized according to the working electrode or counter electrode geometry. The PDMS lid covers only the electrode area of the HECL chip, leaving the electrical contact pads exposed.

2.5. Hydrophobic sample confinement

Hydrophobic sample confinement on HECL electrode chips was effected by depositing a hydrophobic fluoropolymer film in the area around the electrodes. After masking the working and counter electrode areas as well as the electrical contact pads with photoresist, the fluoropolymer film was deposited by the same plasma process as on the SU-8 master in Section 2.4, and patterned by lift-off in acetone. The electrodes were thus left uncoated and hydrophilic, whereas the surrounding areas were left strongly hydrophobic.

2.6. HECL-measurements

A solution of Tb(III) chelated by 2,6-bis[N,N-bis(carboxymethyl)aminomethyl]-4-benzoylphenol was used as the model analyte. HECL measurements were performed in a sample holder with a photomultiplier tube for optical detection and a 550 nm wavelength 40 nm bandwidth optical interference filter to pass only the spectral line emitted by the Tb(III) chelate. Front and backside electrical contacts were provided in the sample holder to interface the HECL chip with an in-house built coulostatic pulse generator described in [25]. Since the pulse generator operates using constant voltage, and adjusts pulse length to compensate for variation in electrical current, an indication of electrical conductance within the HECL chip could be obtained by monitoring the pulse lengths with an oscilloscope. To tunnel inject a controlled charge through the dielectric, 12.6 μC coulostatic pulses were applied at 25 V between the on-chip electrodes at a rate of 20 Hz, and luminescence data was measured over a total of 1000 pulses. In order to further improve selectivity, optical detection was performed in a time-resolved manner [26], integrating luminescence during 3 ms, following a 50 μs delay.

Devices with PDMS fluidics (Fig. 4, middle) were filled with the sample solution by dipping the chip's inlet end into a drop of sample solution on the surface of a glass plate. The PDMS chamber filled rapidly by capillary force, and complete filling could easily be verified by eye. The total sample volume was limited by the volume of the PDMS chamber, about 2 μl and 15 μl for the 50 μm and 350 μm high fluidic chambers, respectively. Hydrophobically confined samples were pipetted directly onto the electrode chip, until a well-defined, nearly hemispherical drop (Fig. 4, right) was formed within the hydrophobic ring. 100 μl of sample solution was used. Devices without any built-in fluidic structures were mechanically sealed in the sample holder against a circular sample cell made of polytetrafluoroethylene (PTFE), with an o-ring of 7.6 mm diameter (Fig. 4, left) and filled with 0.5 ml of solution.

3. Results and discussion

3.1. Effect of electrode geometry

Table 1 presents measured HECL intensities from various silicon electrode designs, measured using a 10^{-6} mol/dm^3 sample solu-

Table 1
Effect of working and counter electrode areas on the observed HECL signal from silicon electrodes with thermal oxide dielectric. The plain silicon sample was measured using a separate platinum wire as the counter electrode. The analyte was 10^{-6} mol/dm^3 Tb(III) chelate solution.

Electrode type	HECL intensity (10^6 counts)	Working electrode area (mm^2)	Counter electrode area (mm^2)	Area ratio
RING 500	7.70	40.7	2.4	17.3
WIRE 800	7.68	37.7	6.1	6.2
CIRC 200	7.59	38.6	3.4	11.4
Plain Si	5.89	24.6	–	–
CIRC 800	5.23	28.8	13.3	2.2
MESH 200/1000	5.23	30.3	7.7	3.9
MESH 800/1000	3.43	20.6	20.4	1.0
MESH 200/500	3.37	23.2	11.3	2.1
MESH 800/500	1.87	12.7	27.0	0.5
WIRE 200	1.71	42.3	1.5	27.9
MESH 200/200	1.64	14.1	16.2	0.9

tion in the PTFE cell (the electrode geometries are identified by the same designations as in Fig. 2). The table is arranged in order of decreasing intensity. Three very different electrode designs top the list with nearly identical results. On the other hand, similar electrode geometries differing only in their dimensions produce great variation in intensity. Thus, when operated in the PTFE sample cell, the electrode geometry *per se* seems to have little or no effect on device performance. Rather, there is an obvious correlation between the signal intensity and the working electrode area, also given in Table 1. Only two major outliers are evident in the table, "Plain Si" and "WIRE 200". The former is a plain oxidized silicon electrode, measured in a slightly different, 5.6 mm diameter sample holder, using a separate platinum wire counter electrode. It is therefore not entirely comparable to the other data, and is included only for reference. The latter has a large working electrode area, but only a small HECL signal is observed, due to its unreasonably small counter electrode. The WIRE geometry itself is not at fault, as shown by the excellent performance of the "WIRE 800" device. Although a large counter electrode should be beneficial as well, the total surface area of the device is, in practice, limited. There must therefore be some optimal ratio of working electrode to counter electrode areas. In this work, best results were obtained with ratios between 5:1 and 20:1. Glass devices exhibited similar trends as the silicon devices.

When 350 μm high PDMS fluidics or hydrophobic sample confinement were employed, the effect of electrode geometry became more critical. The simple RING-type electrodes, while most efficient (7.7×10^6 photon counts) in the PTFE sample cell, produced hardly any signal at all in a PDMS fluidic chip. A MESH 200/1000-type electrode, on the other hand, produced 1.1×10^6 counts in a PDMS fluidic chip—nearly an oder of magnitude lower signal, but still sufficiently high for practical use, considering the low detection limits and great dynamic range of the devices (see Section 3.4). Also in the hydrophobically confined version, the RING electrode's performance was reduced, and a MESH 200/1000 electrode was used instead, producing a signal of 1.5×10^6 counts, comparable to that of the PDMS device. The reason for the MESH electrode's better performance in these instances is presumably increased electrical resistance within the sample solution itself: in the large-volume PTFE sample cell, the sample solution forms a relatively thick layer with correspondingly low resistance between the electrodes, and maximizing the working electrode area has the greatest effect on signal intensity. In the PDMS chamber, however, the solution forms a film only 350 μm thick, with correspondingly higher resistance within the solution. Increased electrical pulse lengths from the coulostatic pulse generator, observed during the measurement, support this explanation.

3.2. Uniformity of electrochemiluminescence

When an electrical pulse is applied to the device, a voltage across the dielectric film causes the tunneling of electrons. A voltage drop also occurs in the sample solution, due to its electrical resistance, and becomes greater as distance from the counter electrode increases. Since this voltage drop is effectively subtracted from the voltage across the dielectric, electron tunneling should decrease as distance from the counter electrode increases, consequently confining electrochemiluminescence to the vicinity of the counter electrode's edge. To verify this, and to investigate the uniformity of luminescence from different electrode designs, long-exposure photographs were taken of devices in normal operation with a 10^{-5} mol/dm^3 sample solution. A Canon EOS 1Ds Mark-II digital camera with a 50 mm f/1.8 lens and 20 mm extension tube was used to image the devices at ISO 1600 sensitivity and 60 s exposure time. A dark frame was subtracted from the raw image, and image brightness was normalized.

A WIRE 800-type device is used to demonstrate the intensity distribution over the working electrode (a RING type's counter electrode is obscured from camera view by the PTFE sample cell). Fig. 5A and B shows the device operating in the PTFE sample cell and with an integrated PDMS fluidic chip, respectively. The luminescence from within the PTFE sample cell is remarkably uniform, due to the thick and low-resistance sample layer as discussed above. The PDMS fluidic device's luminescence, on the other hand, is concen-

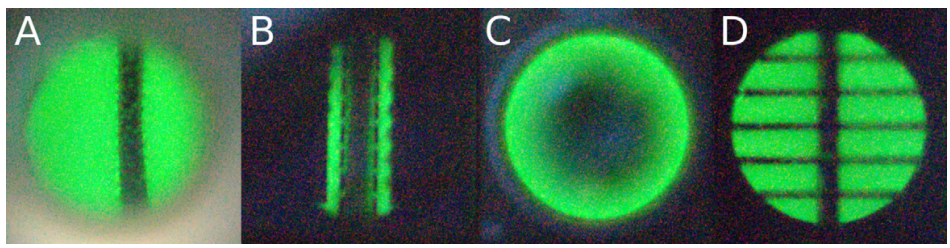

Fig. 5. Long-exposure photographs of various devices using 10^{-5} mol/dm^3 sample solution. (A) WIRE 800 device in PTFE sample cell. (B) WIRE 800 device with PDMS fluidics. (C) RING 500 device with hydrophobic confinement. (D) MESH 200/1000 device with PDMS fluidics.

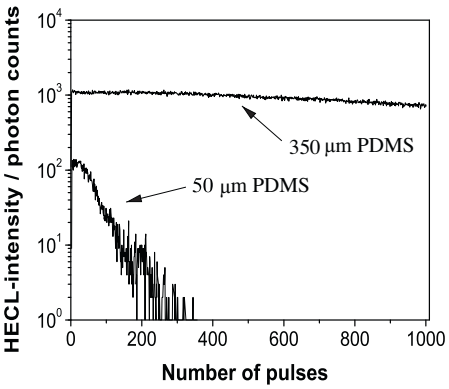

Fig. 6. HECL signal intensity over the course of a measurement of a MESH 200/1000 device with 350 μm (upper) and 50 μm (lower) PDMS sample chambers.

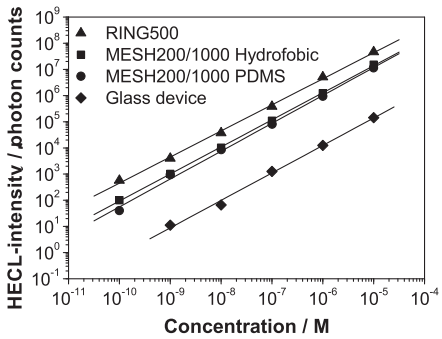

Fig. 7. Calibration curves for Tb(III) chelate using, from top to bottom, a RING 500 device in a PTFE sample cell, a MESH 200/1000 device with hydrophobic sample confinement, a MESH 200/1000 device with PDMS fluidics, and a glass device in a PTFE sample cell.

trated around the counter electrode, as expected due to the sample solution's resistance. Some non-uniformity caused by the PDMS lid's support pillars is also evident in the latter image.

The reduction of the RING-type electrode's performance in its hydrophobically confined version is also evident in the photographs. While the RING electrode was photographically confirmed to have excellent uniformity over its entire surface when operated in the PTFE sample cell, its hydrophobically confined version shows diminished luminescence in the central part of the electrode, far from the surrounding counter electrode (Fig. 5C).

A MESH design was therefore selected for further development in both the integrated PDMS fluidic devices and devices with hydrophobic sample confinement. Two different densities of mesh, with 500 μm and 1000 μm line spacing, were tested. The MESH 200/1000 electrode design (*i.e.* 200 μm wide counter electrode lines at 1000 μm spacing) was found to be more efficient in the PDMS fluidic device, and Fig. 5D confirms its emission to be also highly uniform. A slight improvement in luminescence efficiency might still be possible by increasing the counter electrode's line spacing to the point where luminescence uniformity is just beginning to degrade, but this design should be reasonably near optimal.

Surprisingly, Fig. 5D shows no sign of the support pillars of the PDMS lid, which should be expected to show up dark in the image. Microscope examination reveals the bottoms of the relatively tall but narrow pillars to be imperfectly formed in the molding process of the PDMS lid, and therefore they do not bond hermetically to the surface of the electrode chip. Thus the sample solution is able to penetrate underneath them, and luminescence occurs normally. Only in the case of a strong sideways voltage gradient, as in the WIRE 800 electrode of Fig. 5B, decreased luminescence is observed in the thin sample film under the pillars, due to increased resistive voltage drops in the solution.

3.3. Effect of the PDMS lid

PDMS fluidic systems were fabricated in two heights, 50 μm and 350 μm, and both were tested in silicon MESH-type devices. The 50 μm high devices produced virtually no signal with any electrode geometries. While a thinner film of sample solution may certainly aggravate the effects of resistive voltage drops and thus decrease electron tunneling and luminescence, the primary reason for the poor performance is formation of gas bubbles at the electrodes. After measurement, the 50 μm high fluidic chips were observed to be largely empty of liquid, purged by the action of bubble formation. Some evidence of bubble formation was seen also in other devices (*e.g.* along the counter electrode of the device in Fig. 5A), but their larger sample volumes are able to accommodate some bubbles without deterioration.

In fact, a significant HECL signal was briefly observed also in the 50 μm high PDMS devices immediately at the beginning of the measurement. The signal was, however, an order of magnitude lower than in the 350 μm high PDMS device, and the signal began immediately to fall, decreasing by an order of magnitude after only 100 measurement pulses, as gas bubbles built up. Fig. 6 demonstrates this by showing the luminescence data from individual measurement pulses in both 50 μm and 350 μm high PDMS devices, using MESH 200/1000 electrodes. As the signal intensity of the former fell, electrical pulse lengths simultaneously increased, an indication of increasing electrical resistance within the HECL chip due to accumulation of bubbles. The 350 μm PDMS device, on the other hand, maintained nearly constant signal intensity throughout the 1000 measurement pulses.

3.4. Analytical performance of the devices

Fig. 7 presents calibration curves measured for the model analyte using four different configurations of the HECL devices: A RING 500 device operated in the PTFE sample cell, a MESH 200/1000 device with hydrophobic sample confinement, a MESH 200/1000 device with 350 μm high PDMS fluidics, and a glass device similar to the RING 500 design, also operated in the PTFE sample cell. The electrode geometries were selected for highest possible HECL signal, as presented in Section 3.1. The 50 μm high PDMS chambers were no longer used at this point.

All devices presented in Fig. 7 offer excellent linearity over four to five orders of magnitude, and have detection limits in the subnanomolar range. The upper limit of the calibration curve is set by saturation of the photomultiplier tube. Since no non-linearity is observed prior to this limit, the HECL method itself may well be linear to even higher concentrations.

Immediately obvious in Fig. 7 is the extremely similar performance of all three versions of the silicon device. The RING 500 device with a separately assembled PTFE sample chamber offers best performance, but only by a narrow margin to the hydrophobically confined and PDMS capillary-filling devices. The latter two, however, have the advantage of less assembly and thus shorter analysis time, and no cross-contamination of sample solutions. Especially the PDMS version shines in its exceptionally small requirement for sample volume (15 μl). Evaporation of aqueous samples during measurement is negligible at room temperature, since the HECL measurement itself takes only minutes to run,

much less if fewer integrated measurement pulses will suffice. The hydrophobic sample confinement scheme might, however, be exploited for preconcentration of samples by deliberate evaporation of the solution prior to measurement.

The glass device with its deposited working electrode and tunneling dielectric is seen to have substantially lower sensitivity than the silicon devices, but it still has excellent linearity and attains nanomolar detection limits. Since a deposited dielectric is used, other metals could also be used as the electrode. Using platinum in both the working and counter electrodes would simplify device fabrication, but might slightly degrade device performance, as the choice of electrode metal has been found to greatly affect the intensity and stability of the obtained HECL signal [12]. Alternative tunneling dielectrics could also be utilized. Especially silicon dioxide deposited by plasma-enhanced chemical vapor deposition is an excellent material [12], but in this work the ALD method was preferred due to its better repeatability in producing ultra-thin films. The trimethylaluminum-water process has such a wide ALD window, that smooth and electrically high-quality films can be deposited at temperatures as low as 33 °C [27]. Thus many plastic materials might also be suitable for the production of low-cost disposable devices by technologies such as roll-to-roll processing, hot embossing, or injection molding of fluidic systems.

Previous studies of HECL *e.g.* [11,12] have used planar, unpatterned working electrodes with a separate platinum wire as the counter electrode. While such electrodes are certainly the most economical to manufacture, they do not offer the convenience of the integrated electrode design: disassembly, cleaning and reassembly of the sample cell and counter electrode wire take several minutes between each analysis, whereas an integrated HECL chip can be replaced in just seconds. What is equally important, is that the integration of counter electrodes and fluidic confinement on the chip does not unreasonably degrade analytical performance compared to the planar design. The "Plain Si" entry included for reference in Table 1 demonstrates this. It is measured in a differently designed and smaller sample cell, but assuming all other things equal and linear scaling of intensity with working electrode area, its intensity should be on the order of 9.7×10^6 counts when scaled to the surface area of the RING 500 electrode. That is only barely higher than the RING 500 electrode's intensity in the PTFE sample cell (7.7×10^6 counts). The best devices (with MESH 200/1000 electrode design) with hydrophobic sample confinement and PDMS fluidics exhibit somewhat lower intensities (1.5×10^6 and 1.1×10^6 counts, respectively), but these are still entirely reasonable values especially in applications where ultimate sensitivity is not paramount.

4. Conclusions

We have demonstrated an integrated microfluidic system for quantitative analysis based on hot electron-induced electrochemiluminescence, combining both the working and counter electrodes and sample containment on a single disposable chip. Excellent linearity and sub-nanomolar detection limits were demonstrated with the model analyte.

Three schemes for sample containment were investigated, including a separately assembled PTFE sample cell, integrated PDMS sample chambers and hydrophobic sample confinement. Optimal electrode geometries were presented for each sample containment scheme, and the uniformity of electrochemiluminescence in each was investigated. For luminescence efficiency, maximal working electrode area was found to be most important, but in the PDMS and hydrophobic versions a sufficiently dense mesh-type counter electrode was required to maintain uniform luminescence over the electrode.

While the capillary-filling PDMS fluidic system presented here is simple, it is already a useful device in itself, as it reduces analysis time and eliminates the possibility of sample cross-contamination. Furthermore, the current PDMS fluidic system serves as a proof-of-concept, demonstrating the capability of HECL detection for integration into other microfluidic systems. Hydrophobic sample confinement utilizing plasma-deposited fluoropolymer films, on the other hand, is more economical for mass production, as all processing steps are done on the wafer scale.

HECL devices were fabricated not only on silicon, but also glass substrates, using aluminum thin film electrodes coated with ALD alumina. This demonstrates the feasibility of using insulating substrates and low-temperature processing for HECL devices. Both types of integrated microelectrode device exhibited performance comparable to planar working electrodes with a separate platinum wire counter electrode, used in previous work. The success of glass devices suggests the possibility of using other insulating materials as well, *e.g.* plastic substrates, which are low-cost and provide many interesting options for the production of fluidic systems.

References

[1] M.J. Bronskill, R.K. Wolff, J.W. Hunt, Picosecond pulse radiolysis studies. I. The solvated electron in aqueous and alcohol solutions, J. Chem. Phys. 53 (1970) 4201–4210.

[2] R.K. Wolff, M.J. Bronskill, J.W. Hunt, Picosecond pulse radiolysis studies. II. Reactions of electrons with concentrated scavengers, J. Chem. Phys. 53 (1970) 4211–4215.

[3] Y. Muroya, M. Lin, Z. Han, Y. Kumagai, A. Sakumi, T. Ueda, Y. Katsumura, Ultrafast pulse radiolysis: a review of the recent system progress and its application to study on initial yields and solvation processes of solvated electrons in various kinds of alcohols, Radiat. Phys. Chem. 77 (2008) 1176–1182.

[4] A. Migus, Y. Gauduel, J.L. Martin, A. Antonetti, Excess electrons in liquid water: first evidence of a prehydrated state with femtosecond lifetime, Phys. Rev. Lett. 58 (1987) 1559–1562.

[5] R. Laenen, T. Roth, A. Laubereau, Novel precursors of solvated electrons in water: evidence for a charge transfer process, Phys. Rev. Lett. 85 (2000) 50–53.

[6] S. Kulmala, T. Ala-Kleme, L. Heikkilä, L. Väre, Energetic electrochemiluminescence of (9-fluorenyl)methanol induced by injection of hot electrons into aqueous electrolyte solution, J. Chem. Soc. Faraday Trans. 93 (1997) 3107–3113.

[7] S. Kulmala, T. Ala-Kleme, H. Joela, A. Kulmala, Hot electron injection into aqueous electrolyte solution from thin insulating film-coated electrodes, J. Radioanal. Nucl. Chem. 232 (1998) 91–95.

[8] S. Kulmala, K. Haapakka, Mechanism of electrogenerated luminescence of terbium(III)-2,6-bis[N,N-bis(carboxymethyl)aminomethyl]-4-benzoylphenol chelate at an oxide-covered aluminium electrode, J. Alloys Compd. 225 (1995) 502–506.

[9] G.V. Buxton, C.L. Greenstock, W.P. Helman, A.B. Ross, Critical review of rate constants for reactions of hydrated electrons, hydrogen atoms and hydroxyl radicals ($^{\bullet}OH/^{\bullet}O^{-}$) in aqueous solution, J. Phys. Chem. Ref. Data 17 (1988) 513–886.

[10] T. Ala-Kleme, P. Mäkinen, T. Ylinen, L. Väre, S. Kulmala, P. Ihalainen, J. Peltonen, Rapid electrochemiluminoimmunoassay of human C-reactive protein at planar disposable oxide-coated silicon electrodes, Anal. Chem. 78 (2006) 82–88.

[11] A.J. Niskanen, T. Ylinen-Hinkka, S. Kulmala, S. Franssila, Ultrathin tunnel insulator films on silicon for electrochemiluminescence studies, Thin Solid Films 517 (2009) 5779–5782.

[12] A.J. Niskanen, T. Ylinen-Hinkka, M. Pusa, S. Kulmala, S. Franssila, Deposited dielectrics on metal thin films using silicon and glass substrates for hot electron-induced electrochemiluminescence, Thin Solid Films 519 (2010) 430–433.

[13] T.-K. Shih, C.-F. Chen, J.-R. Ho, F.-T. Chuang, Fabrication of PDMS (polydimethylsiloxane) microlens and diffuser using replica molding, Microelectron. Eng. 83 (2006) 2499–2503.

[14] F. Schneider, J. Draheim, R. Kamberger, U. Wallrabe, Process and material properties of polydimethylsiloxane (PDMS) for optical MEMS, Sens. Actuators A 151 (2009) 95–99.

[15] J.C. McDonald, G.M. Whitesides, Poly(dimethylsiloxane) as a material for fabricating microfluidic devices, Acc. Chem. Res. 35 (2002) 491–499.

[16] M. Zimmermann, P. Hunziker, E. Delamarche, Autonomous capillary system for one-step immunoassays, Biomed. Microdevices 11 (2009) 1–8.

[17] X. Huang, J. Ren, On-line chemiluminescence detection for isoelectric focusing of heme proteins on microchips, Electrophoresis 26 (2005) 3595–3601.

[18] H. Qiu, J. Yan, X. Sun, J. Liu, W. Cao, X. Yang, E. Wang, Microchip capillary electrophoresis with an integrated indium tin oxide electrode-based electrochemiluminescence detector, Anal. Chem. 75 (2003) 5435–5440.

[19] J. Liu, J. Yan, X. Yang, E. Wang, Miniaturized tris(2,2′-bipyridyl)ruthenium(II) electrochemiluminescence detection cell for capillary electrophoresis and flow injection analysis, Anal. Chem. 75 (2003) 3637–3642.

[20] Y. Du, H. Wei, J. Kang, J. Yan, X. Yin, X. Yang, E. Wang, Microchip capillary electrophoresis with solid-state electrochemiluminescence detector, Anal. Chem. 77 (2005) 7993–7997.
[21] Y.-T. Hsueh, S.D. Collins, R.L. Smith, DNA quantification with an electrochemiluminescence microcell, Sens. Actuators B 49 (1998) 1–4.
[22] C. Zhang, D. Xing, Miniaturized PCR chips for nucleic acid amplification and analysis: latest advances and future trends, Nucleic Acids Res. 35 (2007) 4223–4237.
[23] C. Zhang, D. Xing, Micropumps, microvalves and micromixers within PCR microfluidic chips: advances and trends, Biotech. Adv. 25 (2007) 483–514.
[24] S. Kulmala, T. Ala-Kleme, A. Kulmala, D. Papkovsky, K. Loikas, Cathodic electrogenerated chemiluminescence of luminol at disposable oxide-covered aluminum electrodes, Anal. Chem. 70 (1998) 1112–1118.
[25] S. Kulmala, M. Håkansson, A.-M. Spehar, A. Nyman, J. Kankare, K. Loikas, T. Ala-Kleme, J. Eskola, Heterogeneous and homogeneous electrochemiluminoimmunoassays of hTSH at disposable oxide-covered aluminum electrodes, Anal. Chim. Acta 458 (2002) (2002) 271–280.
[26] M. Håkansson, Q. Jiang, M. Helin, M. Putkonen, A.J. Niskanen, S. Pahlberg, T. Ala-Kleme, L. Heikkilä, J. Suomi, S. Kulmala, Cathodic Tb(III) chelate electrochemiluminescence at oxide-covered magnesium and n-ZnO:Al/MgO composite electrodes, Electrochim. Acta 51 (2005) 289–296.
[27] M.D. Groner, F.H. Fabreguette, J.W. Elam, S.M. George, Low-temperature Al_2O_3 atomic layer deposition, Chem. Mater. 16 (2004) 639–645.

Biographies

Antti J. Niskanen received his Master's degree in Chemical Engineering in 2002 from the Helsinki University of Technology, on the subject of liquid phase deposition of silicon dioxide thin films. He currently works in the Microfabrication Group of the Department of Micro and Nanosciences, and is working on his doctoral thesis. He has worked on the fabrication aspects of microhotplate gas sensors, and his current research interests center around thin film technology for electrochemiluminescent sensors.

Tiina Ylinen-Hinkka got her M.Sc. in 2004 from the laboratory of Analytical Chemistry at the University of Turku. At the moment, she is doing her Ph.D. studies in the laboratory of Analytical Chemistry at Aalto University School of Science and Technology. Her research is mainly focused on different kinds of cathode materials and insulating layers suitable for hot electron induced electrochemiluminescence (HECL) in macro and micro analysis systems. She is also interested in biomedical applications of HECL. Before starting her Ph.D. studies, she has worked as a teacher.

Sakari Kulmala, Ph.D., is the Professor of Analytical Chemistry at the Helsinki University of Technology since 1. 9. 1999, and the director of the Graduate School of Chemical Sensors and Microanalytical Systems (CHEMSEM) in 2002–2009.

Sami Franssila studied physics and chemistry at the University of Helsinki and obtained B.Sc. and M.Sc. degrees in 1985 and 1986. His Ph.D. degree is from from Helsinki University of Technology, School of Electrical Engineering (1995) with a thesis on plasma etching. He worked as a research scientist at VTT Microelectronics from 1986 till 1998, with 1993–1994 at IMEC, Belgium, and since 1998 at Helsinki University of Technology. He has worked on CMOS, MEMS and microfluidic devices and has published 80 peer reviewed journal articles and a textbook "Introduction to Microfabrication". He is currently a Professor of Materials Science, with research interests in materials and fabrication technologies for fluidic, bio, chemical and thermal devices, and flexible electronics.